An experimental and predictive study of the flow field in axisymmetric automotive exhaust catalyst systems

Benjamin, S.F. , Clarkson, R.J. , Haimad, N. and Girgis, N.S.

SAE TECHNICAL
PAPER SERIES

961208

An Experimental and Predictive Study of the Flow Field in Axisymmetric Automotive Exhaust Catalyst Systems

S. F. Benjamin, R. J. Clarkson, N. Haimad, and N. S. Girgis
Coventry Univ.

SAE The Engineering Society For Advancing Mobility Land Sea Air and Space®
INTERNATIONAL

International Spring Fuels
& Lubricants Meeting
Dearborn, Michigan
May 6-8, 1996

400 Commonwealth Drive, Warrendale, PA 15096-0001 U.S.A. Tel: (412)776-4841 Fax:(412)776-5760

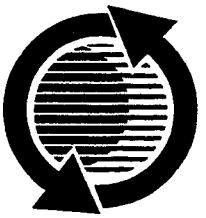

ISSN 0148-7191

Printed in USA 96-0049

961208

An Experimental and Predictive Study of the Flow Field in Axisymmetric Automotive Exhaust Catalyst Systems

S. F. Benjamin, R. J. Clarkson, N. Haimad, and N. S. Girgis
Coventry Univ.

ABSTRACT

An experimental and theoretical investigation has been performed on the flow and pressure loss in axisymmetric catalytic converters and isolated monoliths under steady, isothermal flow conditions. Monolith resistance has been measured with a uniform, low turbulence, incident flow field. It has been found that the pressure loss expression for fully developed laminar flow is a good approximation to observations for x^+ greater than 0.2. However, for x^+ less than 0.2 the additional pressure loss due to developing flow is no longer negligible and a better approach is to use the correlation proposed by Shah (16). From experimental studies on the axisymmetric catalytic converters non-dimensional power law relationships have been derived relating maldistribution and pressure drop to expansion length, *Re*, and monolith length. These expressions are shown to generally fit the data well within ±5%. CFD predictions of the flow for a wide range of geometric configurations and flow conditions have shown that generally the system non-dimensional pressure loss can be predicted to within about 10% but that the maldistribution index is underpredicted within a range of 9-17.5%. It is believed that the pressure loss expression derived from 1-D flow studies is too simplistic. CFD predictions do, however, show the same pattern of change as observed experimentally and hence their performance in predicting trends is quite encouraging.

NOMENCLATURE

d	width of a monolith channel
D_i	diameter of inlet pipe
D_o	outlet diameter of diffuser
f	friction factor
L	monolith length
L_d	diffuser length
M	maldistribution index
ΔP_s	static pressure loss across catalyst
ΔP_t	total pressure loss across catalyst
Rc	Reynolds number (monolith channel)
Re	Reynolds number (inlet pipe)
U_c	mean channel velocity
U_{in}	mean velocity in inlet pipe
U_{max}	maximum velocity at rear of monolith
U_{mean}	mean velocity at rear of monolith
x	distance along monolith
x^+	$(x/Rc\ \mathrm{d})$ non-dimensional distance
ε	monolith porosity (void fraction)
ρ	air density

INTRODUCTION

It has been known for some time that the performance of automotive catalytic converters is affected by the flow distribution within the monolith. Early theoretical and experimental studies (1-3) showed that poor flow distribution within the substrate can reduce catalyst longevity by locally 'wearing out' the precious metal coatings whilst causing a deterioration in emissions. Poor flow distribution is also indicative of higher system pressure losses which implies reduced engine performance and a deterioration in fuel economy. Equally important is the fact that large sections of the monolith are effectively by-passed causing inefficiency in precious metal utilisation leading to increased product costs.

The reasons for poor flow distribution in catalyst monoliths is due to a combination of factors. Flow losses in monoliths are essentially proportional to their length and hence for a given catalyst volume short substrates of large frontal area would seem desirable. This requires a large expansion from the exhaust pipe through a diffuser to the monolith. Packaging constraints usually do not

allow for optimum diffuser design and normally this expansion takes place over a relatively short distance. This results in flow separation from the diffuser walls leading to a maldistributed flow within the brick. The inlet conditions at entry to the diffuser can also greatly affect its performance and the nature of the upstream pipework (again largely governed by packaging constraints) is critical. With the tendency to move towards close coupled catalysts these problems are becoming more acute and the need to assess the flow conditions within these systems is becoming more important. Whilst it is recognised that a considerable body of information is available on the performance of open diffusers there is little to guide the design engineer on diffusers featuring large downstream resistances. The monolith will reduce the degree of flow non-uniformity at the expense of pressure loss. It is clearly desirable to be able to quantify these effects.

It is now becoming practise within the automotive industry to establish criteria for flow distribution within the converter. Engineers faced with designing converters to meet such criteria are largely relying on flow bench studies and more recently, computational fluid dynamics (CFD) (4-6) to assess the performance of proposed systems. The latter approach, whilst offering the prospect of reducing development time, remains unproven for this type of application and validation is still necessary. Also, although some work has been published on flow distribution in catalysts (7-11), there is still only a limited amount of information to guide designers on the choice of systems and, importantly, on the effect of various system parameters on flow performance.

With this in mind a programme of work has been undertaken at Coventry University with the following objectives:

(1) To study the effect of catalyst geometry and inlet flow on the pressure loss and flow maldistribution in axisymmetric steady flow isothermal systems and

(2) To assess the performance of CFD codes in predicting flow behaviour in such systems.

The studies have focused on axisymmetric systems for several reasons. Firstly, these systems are expected to contain many of the important primary flow features associated with more complex geometric configurations- i.e. separated flows with large recirculation. Secondly, the nature of the flow can also be more readily obtained as fewer measurements are needed to characterise the systems (the flow is two dimensional) and thirdly, the computational resources needed to simulate 2-D regimes are far less demanding. Finally it is believed that focusing on simple axisymmetric configurations will aid in the understanding of the relationships between the various controlling parameters and also in the design of more complex systems. To date, studies have been confined to steady flows. Apart from the obvious practical advantages from an experimental and computational point of view it is expected that for many underbody systems flow field pulsations will be of secondary importance. Also, whilst not proven, it is reasonable to assume that in many instances the influence of many of the controlling parameters for steady flow would be similar to pulsating flow environments. Further, when considering the application and validation of CFD techniques, it would seem useful to first ensure that the codes perform well under steady flow conditions before embarking on pulsating flow studies.

ISOTHERMAL STEADY FLOW RIG

AXISYMMETRIC SYSTEMS-A full description of the rig and test procedures is given by Clarkson (12). Figure 1 shows a schematic of the flow rig as used for the 2D studies. The rig air supply was taken from a compressed air system. The system is fed from two large receiver tanks that are rated up to pressures of 30 bar. The particular limb of the system to which the rig was attached has a "Wizard" control valve between it and the receiver tanks, the purpose of which is to provide a constant downstream pressure from varying upstream pressures. A gate valve was provided to allow fine adjustment so as to achieve a constant flow rate. A viscous flow meter was included so that a known flow rate could be passed through the rig and it could be established that the flow rate was not changing. Its presence also meant that a comparison could be made between it and the flow rate given by integrating the velocity profiles measured at the rear of the monolith.

The working section comprised of an inlet pipe, inlet expansion, monolith and outlet section. One of the main design specifications for the working section was that boundary conditions would be known and could be set up within the mathematical model using standard CFD techniques. For this reason a straight upstream pipe was provided (50 diameters) to produce a fully developed velocity profile. A proprietary make of extruded PVC pipe was used of designated diameter 55mm. The inlet expansion comprised of a selection of conical diffusers of total angles (twice the wall angle) of 80°, 60°, 40°, 30°, 20° and 10°. For cost reasons and ease of manufacture these diffusers were machined from wood (Jelutong) and were finished so as to make them hydrodynamically smooth. Velocity profiles were measured with a pitot tube by making a radial traverse downstream of the monolith. To facilitate such measurements no outlet cone was attached to the catalyst assembly, which consequently exhausts, almost directly to atmosphere. The jets that emerge from each monolith channel create a velocity profile across the exit plane of the monolith that consists

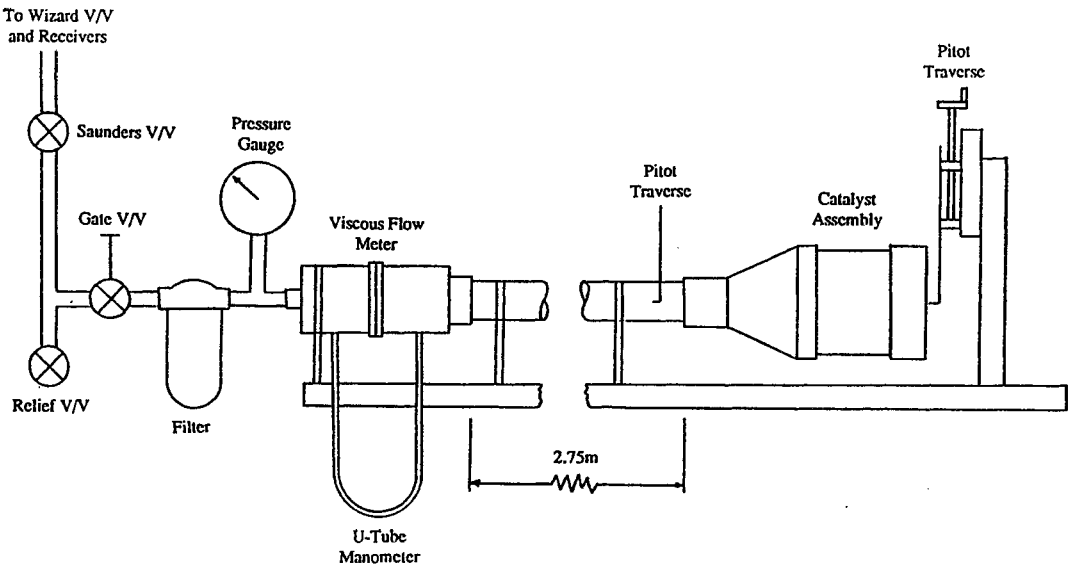

Figure 1: The experimental flow rig.

of a series of peaks and troughs. At 30mm away from the monolith the jets have mixed to such an extent that the velocity profiles appear smooth. Thus it was decided to measure the monolith velocity profile 30mm from its rear face. To prevent entrainment of surrounding air by the jets emerging from the peripheral channels a 30mm outlet sleeve was provided. The pitot traverse was made flush with the exit plane of the sleeve. The ceramic monoliths used for the 2D studies were unwashcoated in order to reduce uncertainty over channel dimensions and shape. The monoliths varied in length but otherwise were nominally the same cell density featuring square sectioned channels. A summary of components is given in table 1.

The data sets reported here comprise of the above mentioned velocity profile and the static and total pressure drop across the catalyst assembly. The velocity profile was measured with a pitot tube of internal diameter of approximately 0.5mm supported on a lead screw based traversing mechanism. For measurements of pressure loss wall static pressure tappings were formed by fitting 1 mm diameter capillary tubes into the wall of the inlet pipe 110mm upstream from the inlet expansion throat. At this location three evenly distributed tappings were provided on the same circumference. Static and dynamic pressures were measured using a differential manometer made by Combustion Instruments Ltd (*circa* 1980) with a range of 0 to 300 Pa and a resolution of 0.05 Pa. Based on the manufacturer's specification pressure measurements within ±0.16 Pa would be expected at the 95% confidence level. Air density was

Table 1 Dimensions of rig components.

Component	Dimension	Nominal Size
Inlet Pipe	Length I/D	2.75m 55mm
Inlet Expansion	Inlet I/D Outlet I/D Area Ratio	55mm 116mm 4.448
Monolith	"Wetted" Diameter	116mm
Outlet Sleeve	I/D Length	116mm 30mm

Conical Diffusers	
Total Angle	Nominal Length
80°	37mm
60°	53mm
40°	84mm
30°	114mm
20°	173mm
10°	349mm

Monolith Length (mm)	Channel Breadth (mm)	Void Fraction (%)
102	1.09	70.0
127	1.10	72.5
152	1.10	72.5

derived from the ideal gas law from measurement of the barometric pressure and air temperature and is estimated to be accurate to 0.23% at the 95% confidence level. Hence for *Re*=60000 a mean velocity at the rear of the monolith would be expected to be measured to within 1% at the 95% confidence level. The corresponding figure at *Re*=30000 would be 3.9%.

To check that the inlet velocity profile to the catalyst assembly was fully developed, a pitot traverse was made at the exit from the inlet pipe and the results are shown in figure 2 where comparisons with two other sources of have been made; namely Schlichting(13) and Heitor and Rodrigues(14). It can be seen that the profiles are very close to fully developed flow.

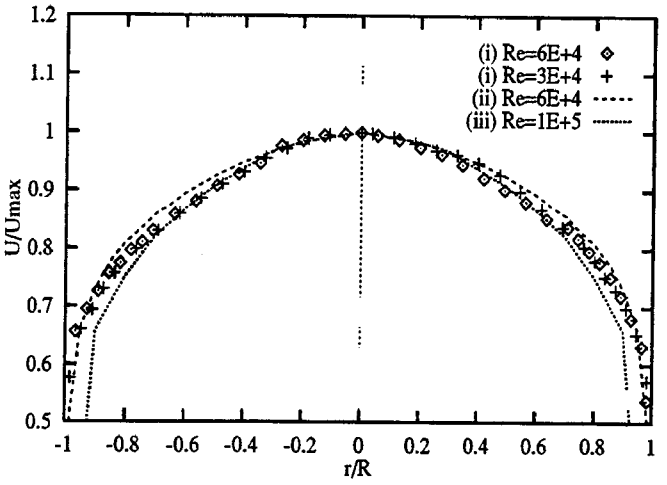

Figure 2: Velocity profiles at the exit to the inlet pipe: (i) Experimental data, (ii) From Schlichting (13), (iii) From Heitor and Rodrigues (14).

As part of the rig commissioning process a brief assessment of the axisymmetric nature of the flow was made by measuring the monolith velocity profiles across two perpendicular diameters. An example of these profiles can be seen in figure 3 and indicates that the flow was close to axisymmetric. Consequently, unless suspicions were raised, in the majority of cases the velocity profile was measured across only one diameter. By carrying out two separate integrations, one for each radius, an indication of the flow symmetry could be obtained. A symmetry error was defined as the difference between the two integrated flow rates divided by the mean of the two. The average symmetry error for the test cases was 2.1%. The average difference between the mass flow rates given by the viscous flow meter and the mean integrated value, expressed as a percentage of the viscous flow meter is 2.4% over all test cases.

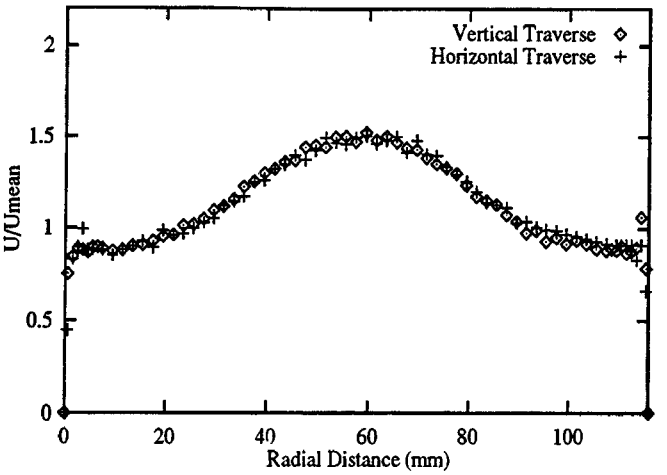

Figure 3: Velocity profiles at rear of the monolith with a 20° diffuser and 152mm monolith at *Re*=61000.

MONOLITH LOSSES-In order to perform CFD simulations (described later) it is necessary to ascertain the flow resistance of the monolith itself. Essentially a relationship is required between flow velocity and pressure drop and this requires a uniform 1D velocity profile at entry to the monolith to ensure that the boundary conditions at each of the monolith channels are identical. This was achieved by designing a contraction nozzle based on a contour that was numerically derived by Borger (15). It features a contraction ratio of 16.5 with an outlet diameter of 48mm. The nozzle was fitted downstream of a straightening section designed to provide unidirectional flow at the inlet to the contraction as well as suppressing any swirl from the air supply. The straightening section consisted of a series of gauzes and tube bundles. The monoliths were flush mounted with the exit plane of the contraction. Static pressure was measured 10mm upstream of the monolith on an inner straight section of the nozzle. Velocities were measured by pitot traverse at the exit to the monolith. A schematic of the arrangement is shown in figure 4. Figure 5 shows the velocity profiles measured at the nozzle exit. For *Re* greater than about 5000 (which corresponds to a channel velocity of under 2m/s) the boundary layers are very thin and a uniform profile is to be expected over the catalyst face. Turbulent intensity at the exit of the nozzle, as measured using hot-wire anemometry, was low; ranging from 0.9 to 1.45%.

Washcoated and unwashcoated monoliths, similar to those used for the 2D studies were tested. The former were specially prepared to provide a relatively uniform coating. Various monolith lengths were tested and with *Rc* ranging from 10 to 1200 (based on the channel

hydraulic diameter and mean channel velocity). Table 2 lists the monoliths tested.

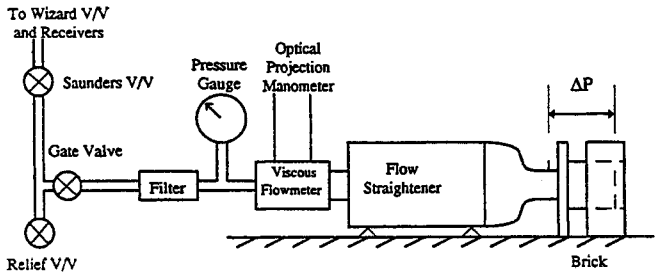

Figure 4: Flow rig with upstream contraction.

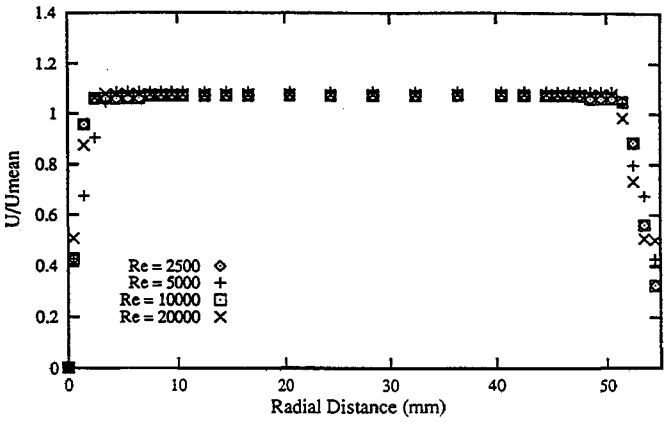

Figure 5: Velocity profiles at the exit plane of the contraction.

A mean dimension of the square channels was obtained from many cell measurements using an optical measuring instrument (Sigmascope VF 600). Instrument specification states an accuracy of ±2μm. The channel breadth (as shown in table 2) was obtained by averaging many cell measurements. The cell density was obtained simply by counting cells. The porosity (ε), of the monoliths was obtained as follows:

$$\varepsilon = \frac{\sum_{i=1}^{i=n} d_i^2}{A}$$ where n is the number of channels in area A .

Table 2 Monoliths for 1D studies.

Monolith Length (mm) unwashcoated	Channel Breadth (mm)	Void Fraction (%)
49	1.11	71.7
74	1.12	71.9
102	1.09	69.0
127	1.11	70.1
washcoated		
49	1.01	61.9
75	1.02	62.2
101	1.00	61.0
125	1.00	58.0

EXPERIMENTAL RESULTS

MONOLITH RESISTANCE-In a channel of a monolith catalytic converter *Rc* is typically less than 1000 and so the flow can be considered laminar. The total pressure drop can be considered as being composed of that due to fully developed flow plus an additional pressure loss due to the developing boundary layer. The relative importance of these two contributions is a function of *Rc* and channel shape. Shah (16) has proposed an expression for the non-dimensional pressure loss as follows:

$$\frac{\Delta P}{\frac{1}{2}\rho U_c^2} = \left(f_{app}Rc\right)\left(4x^+\right) = \left(fRc\right)\left(4x^+\right) + K(x)$$

$$f_{app}Rc = \frac{3.44}{\sqrt{x^+}} + \frac{\left(fRc\right) + K(\infty)\Big/\left(4x^+\right) - 3.44\Big/\sqrt{x^+}}{1 + C\left(x^+\right)^{-2}} \qquad (1)$$

where f_{app} stands for apparent Fanning friction factor which is based on the total pressure loss from x=0 to x. $K(x)$ is an additional dimensionless pressure loss which accounts for the change of momentum flux. $K(x)$ equals zero at the duct inlet and increases to a constant value $K(\infty)$ in the fully developed region. Table 3 summarises the values of the above parameters appropriate for square channels.

Table 3 Constants for laminar flow in square channels.

fRc	*C*	*K*(∞)
14.227	0.00029	1.43

For fully developed flow along the full length of the channel EQ(1) reduces to the Hagen-Poiseuille relationship:

$$\frac{\Delta P_t}{\frac{1}{2}\rho U_c^2} = (fRc)(4x^+) \qquad (2)$$

Figure 6 shows the non-dimensional pressure loss against non-dimensional distance for both washcoated and unwashcoated monoliths. Also plotted are EQs (1) and (2). It can be seen that EQ (1) fits the data well. The Hagen-Poiseuille expression, EQ (2), is seen to be a good fit for x^+ greater than 0.2. The results also suggest that the losses due to channel entrance and exit effects as well as losses in the inlet sections of the nozzle and the outlet sleeve are relatively small.

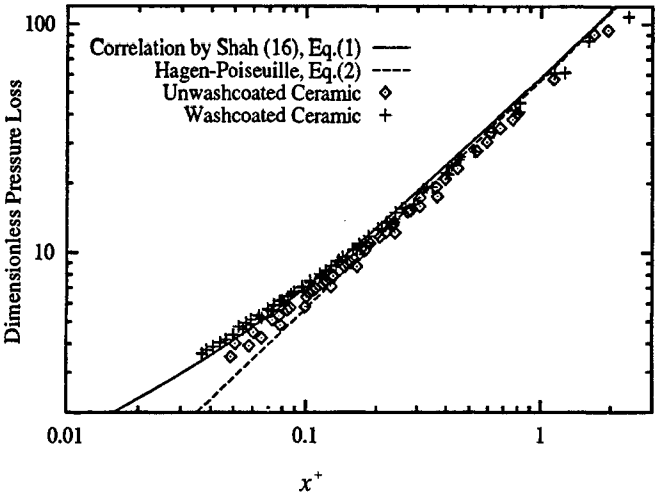

Figure 6: Non-dimensional pressure loss versus non-dimensional distance for washcoated and unwashcoated monoliths.

AXISYMMETRIC SYSTEMS-Tests were performed for a range of configurations as shown in table 4. They were performed at two values of *Re*. Velocity profiles and pressure drop were obtained for each test. A typical velocity profile at the rear of the monoliths is shown in figure 7. The velocities have been non-dimensionalised against the mean outlet velocity derived from the integrated velocity profiles as this was considered the appropriate normalisation when comparing maldistribution indices (see later). Maximum velocities are observed in the central region and local maxima near the periphery. The occurrence of the maximum near the centre line is to be expected. The occurrence of the local maxima at the periphery is due to the fact that near the monolith face a significant radial velocity component (away from the centreline) exists. When this radial flow reaches the diffuser walls, just upstream of the catalyst face, it decelerates causing a locally higher pressure. This local pressure rise near the periphery is the source of the local velocity maxima.

Table 4 Listing of test cases.

Monolith Length(mm)	152		127		102	
Re(x10E-4)	6	3	6	3	6	3
Total Diffuser Angle (Length mm)						
80° (37)	*	*	*	*	*	*
60° (53)	*	*			*	*
40° (84)	*	*			*	*
30° (114)	*	*			*	*
20° (173)	*	*	*	*	*	*
10° (349)	*	*			*	*

* denotes that test case data were obtained.

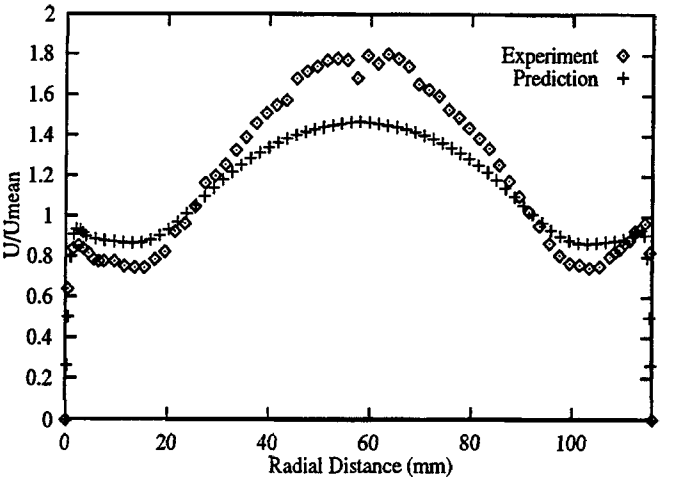

Figure 7: Experimental and predicted (using k-ε RNG and NR models) velocity profiles at rear of monolith for the 80° diffuser, with 152mm monolith, for *Re*=62000.

A method of representing the flow maldistribution is required. A convenient parameter, named the maldistribution index (M), can be defined as follows:

$$M = \frac{U_{max}}{U_{mean}}$$

The non-dimensional static and total pressure drops across the assembly are defined as:

$$\frac{\Delta P_s}{\frac{1}{2}\rho U_{in}^2} \text{ and } \frac{\Delta P_t}{\frac{1}{2}\rho U_{in}^2} \text{ respectively.}$$

The total pressure drop was obtained by adding static pressure to the dynamic pressure-the latter obtained through numerical integration of the mass flow weighted dynamic pressures as obtained from the velocity profiles at inlet and exit of the system.

An instructive way of illustrating the trends in the monolith velocity profiles and the total pressure losses, together, is to plot the flow maldistribution index against the non-dimensional total losses. Such a plot for the diffuser assemblies is shown in figure 8. Note that tentative contours of constant monolith length and diffuser angle have been drawn at the two *Re*'s tested. Figure 8 shows that as diffuser angle increases the flow maldistribution and the pressure drop increase. Increasing the monolith length flattens the velocity profiles by increasing the downstream resistance (and hence pressure loss). The effect of *Re* is quite pronounced. As it increases both the flow maldistribution and total pressure loss increase (N.B. the *non-dimensional* total pressure loss decreases).

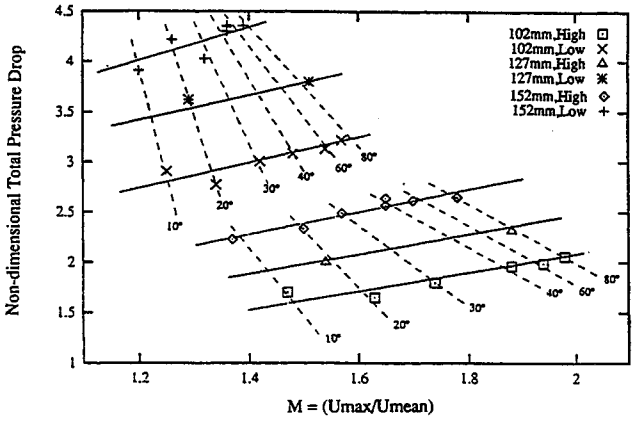

Figure 8: Non dimensional total pressure drop versus maldistribution index for various diffuser angles, monolith lengths and *Re*'s (in key, number of mm refers to monolith length, "High" refers to *Re*=60000, "Low" refers to *Re*=30000, angles refer to diffuser angles).

REPEATABILITY TESTS

Throughout the experimental programme a number of features of the catalyst assemblies were identified that might have caused inconsistencies between the modelling approach (see later) and reality. For example, because diffusers were made of wood their throats had a slight radius on them, in contrast to the computational models which assumed the throats had perfectly sharp corners. In addition it was found that the dimensions of the diffusers varied slightly, by 1 or 2 mm, from those specified in the drawings, and that the "wetted" surfaces were not perfectly smooth. Variations in the internal dimensions of the monoliths can also be expected.

To assess how sensitive results were to these slight variations in assembly geometry two repeatability tests were set up. In the first a duplicate 60° wooden diffuser was made, which, almost inevitably, differed in length from the original by 1.5mm. A different monolith of the same length and nominal cell density was fitted. It was tested at *Re*'s of 60000 and 30000. A comparison of velocity profiles from these tests is shown in figure 9. In the second set of tests a duplicate 40° diffuser was machined from aluminium; the aim being to produce a sharp corner at the throat and a uniform, good quality surface finish on the internal walls. The original monolith was fitted. The velocity profiles for *Re* of 60000 and 30000 are shown in figure 10. It can be seen that overall very good agreement is achieved; there being less

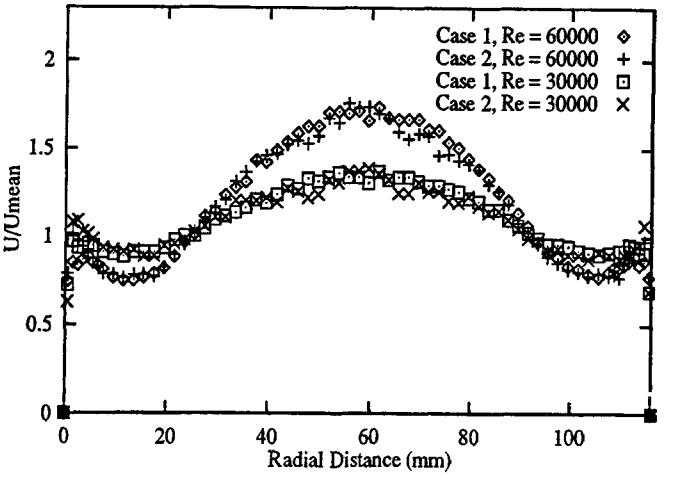

Figure 9: Velocity profiles from two different 60° diffusers with different 152mm monoliths. Case 1 and case 2 refer to the two different assemblies.

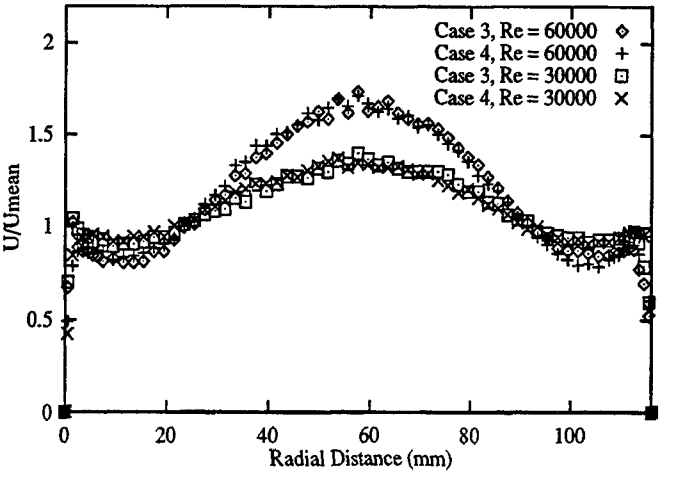

Figure 10: Velocity profiles from two different 40° diffusers using the same 152mm monoliths. Case 3 and case 4 refer to the two different assemblies.

than 3% difference in the maldistribution index between like tests. The non-dimensional total pressures were also measured for the cases shown in figure 10 and they differed by 0.14% and 2.7% for the high and low *Re*'s respectively.

DIMENSIONAL ANALYSIS

It is of interest to examine if general relationships can be derived between the major controlling variables. Such relationships would be useful for determining maldistribution and pressure loss for dynamically similar conditions without the need for conducting further tests. Also such expressions would be useful to design engineers as a starting point when developing similar types of systems.

Restricting ourselves to axisymmetric configurations, conical diffusers and two dimensional isothermal fully developed inlet flow conditions then Buckingham's π theory gives the following functional relationships for flow performance in terms of independent dimensionless groups:

$$M = f_1\left(Re, \frac{L_d}{D_i}, \frac{D_i}{D_o}, \frac{LD_i}{\varepsilon d^2}, \varepsilon\right)$$

$$\frac{\Delta P_t}{\frac{1}{2}\rho U_{in}^2} = f_2\left(Re, \frac{L_d}{D_i}, \frac{D_i}{D_o}, \frac{LD_i}{\varepsilon d^2}, \varepsilon\right)$$

where the functions f_1, f_2 must be derived empirically. The choice of dimensionless groups is not unique. The combinations above are based on physical reasoning as discussed later. For the tests recorded here the ratio of diffuser inlet to outlet diameters (or expansion ratio) was constant and the cell hydraulic diameter and porosity were approximately constant; the major monolith variable being its length, L.

One of the simplest forms of relationship between dimensionless groups would be of the power law type and so it is useful to examine whether such expressions can be derived. Hence the functional relationships reduce to:

$$M = k_1 Re^{a_1}\left(\frac{L_d}{D_i}\right)^{b_1}\left(\frac{LD_i}{\varepsilon d^2}\right)^{c_1}$$

$$\frac{\Delta P_t}{\frac{1}{2}\rho U_{in}^2} = k_2 Re^{a_2}\left(\frac{L_d}{D_i}\right)^{b_2}\left(\frac{LD_i}{\varepsilon d^2}\right)^{c_2}$$

The exponents a_i etc. and constants k_i can readily be determined and the following expressions derived:

$$M = 0.61 Re^{0.31}\left(\frac{L_d}{D_i}\right)^{-0.11}\left(\frac{LD_i}{\varepsilon d^2}\right)^{-0.26} \quad (3)$$

$$\frac{\Delta P_t}{\frac{1}{2}\rho U_{in}^2} = 5.4 Re^{-0.79}\left(\frac{L_d}{D_i}\right)^{-0.074}\left(\frac{LD_i}{\varepsilon d^2}\right)^{0.87} \quad (4)$$

Figures 11 and 12 show plots of experimental values against the empirical expressions EQs (3) and (4). It can be seen that very good agreement is obtained. Generally the difference between experimental and predicted results is much better than ±5%.

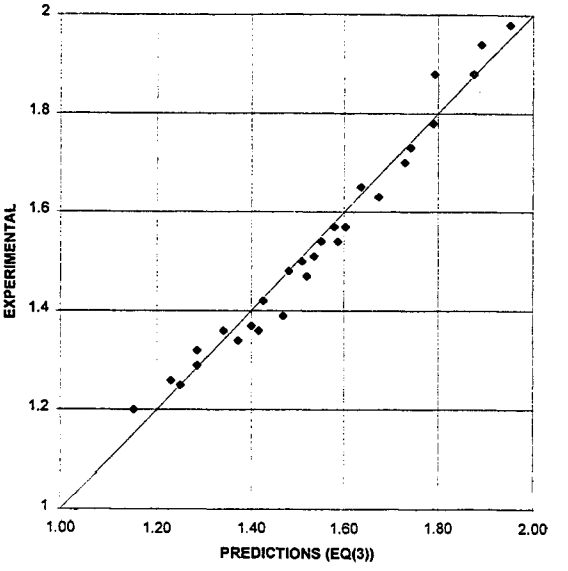

Figure 11: Maldistribution index-experimental versus predicted (EQ (3)).

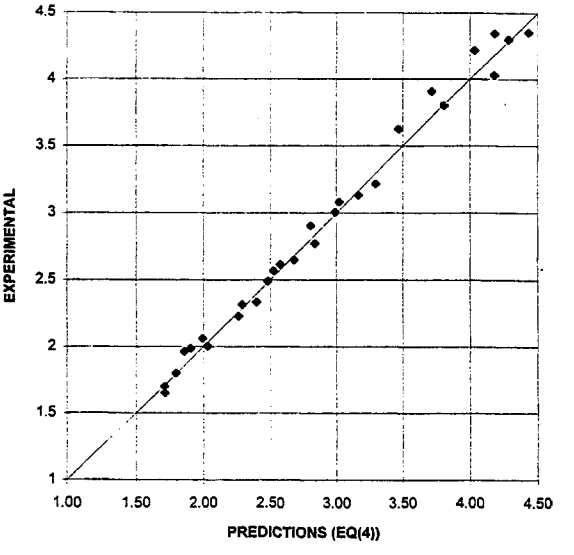

Figure 12: Non-dimensional pressure drop-experimental versus predicted (EQ (4))

A relationship between M and $\Delta P_t / \frac{1}{2}\rho U_{in}^2$ can be established by dividing EQ(4) by (3) giving:

$$\frac{\Delta P_t}{\frac{1}{2}\rho U_{in}^2} = \frac{1}{Re}\left(\frac{LD_i}{\varepsilon d^2}\right)M\left[\frac{8.9}{Re^{0.1}}\left(\frac{LD_i}{\varepsilon d^2}\right)^{0.13}\left(\frac{L_d}{D_i}\right)^{0.036}\right] \quad (5)$$

The above expression can be compared with the Hagen-Poiseuille relationship for monolith losses only assuming uniform fully developed laminar flow within the substrate. It is easy to show that core losses are then given by:

$$\frac{\Delta P_{core}}{\frac{1}{2}\rho U_{in}^2} = \frac{1}{Re}\left(\frac{LD_i}{\varepsilon d^2}\right)\left[2k\left(\frac{D_i}{D_o}\right)^2\right] \quad (6)$$

where k is a constant in the Hagen-Poiseuille equation which for square channels is 28.5. (N.B. this expression is the same as EQ (2)). Hence for a fixed expansion ratio the expression in the square bracket in EQ (6) is constant and may be compared with the equivalent term in EQ (5). In EQ (5) the expression in the square bracket is a relatively weak function of *Re* and catalyst geometry for a given catalyst expansion ratio which suggests that most of the losses are associated with the monolith itself. The functional similarity between EQs (5) and (6) is the reason for choosing the non-dimensional groupings discussed earlier. It could be argued that groupings based around the monolith losses as given in EQ (1) might be more appropriate but the extra complexity and the fact that EQs (3) and (4) perform well suggests that this is unnecessary.

An approximate estimate of the total to core losses can be derived from the ratio of EQs (5) and (6). This ranges from about 1.5 to 1.00 with the highest ratios associated with the widest angle diffusers and highest *Re*.

CFD SIMULATIONS

As noted earlier CFD is now becoming widely used as a technique to simulate flows in catalytic converters. However only a limited amount of validation has been performed. The experimental data described here provides an opportunity to assess CFD codes over a wide range of geometries with well defined inlet conditions.

The code used in this study is STAR-CD. The code is a finite volume code and contains a range of modelling and solver options. A full description of its structure and use can be found in (17). The modelling approach requires the generation of the geometry of the flow domain over which a mesh of computational cells is superimposed. The discretised conservation equations for the field variables (pressure, velocity etc.) are then solved iteratively providing solutions for each cell in the computational domain.

One of the difficulties with simulating the flow field in catalytic converters is that an extremely large number of cells would be required if each channel within the monolith were to be simulated. To overcome this difficulty the monolith is simulated as a porous media wherein the flow is uni-directional and the substrate resistance is prescribed as a function of the local mean channel velocity.

This approach has been described in (12) and (18). In those studies a detailed investigation was made of the effect of grid refinement, differencing scheme and turbulence models in simulating a range of catalyst geometries. Figure 13 shows a typical grid used for the simulations. The grid is two dimensional and the flow domain incorporates the inlet pipe, diffuser housing and substrate. The monolith resistance was simulated by using the Hagen-Poiseuille equation appropriate for square channels i.e. EQ (2). From these studies it was demonstrated that using the k-ε RNG (17) turbulence model gave slightly improved predictions to the standard k-ε model. However far better improvements were achieved with the addition of the Norris-Reynolds (NR) two-layer wall model (19)- this giving far superior results to using wall functions. Even so the maldistribution was underpredicted for the cases considered.

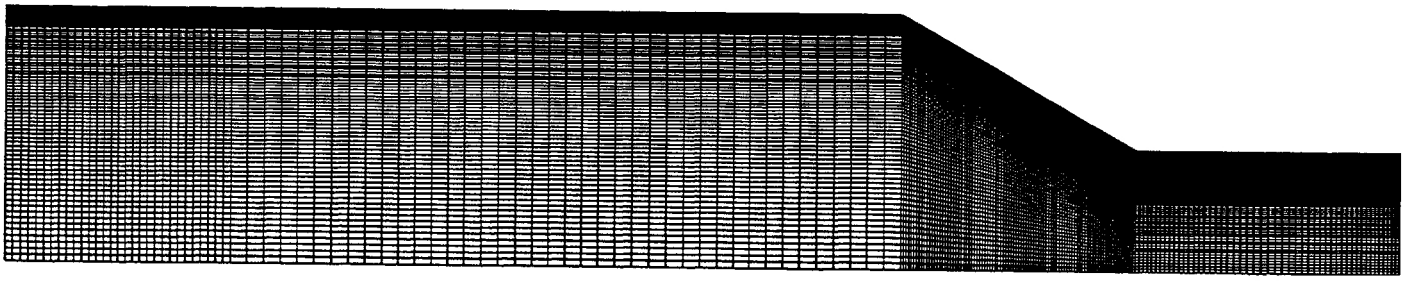

Figure 13: Typical computational grid of an axisymmetric catalyst assembly

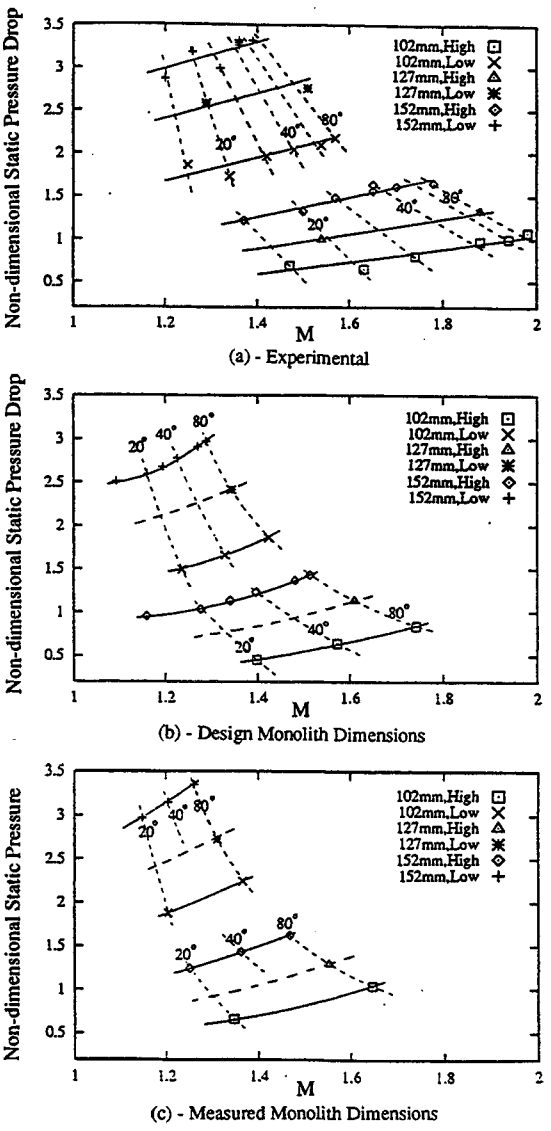

Figure 14: Non dimensional static pressure drop versus maldistribution index diagrams for catalysts with conical diffusers (in key, number of mm refers to monolith length, "high" refers to *Re*=60000,, "Low" refers to *Re*=30000, angles refer to diffuser angles).

A number of simulations adopting the best approach as found in (18) have been undertaken and are shown in figure 14. The simulations were performed using the Norris-Reynolds two layer wall model coupled with the k-ε RNG turbulence scheme. A nominally second order accurate self filtering central difference (SFCD) scheme was used. Mesh refinement was conducted to ensure grid independent solutions were obtained. The results are presented in terms of non-dimensional static pressure drop against maldistribution index. Figure 14b uses the design dimensions of the monoliths i.e. a porosity of 77.8% and a cell width of 1.12mm. Figure 14c uses the values given in table 1. From these diagrams it can be seen that the pattern of the predicted data points is very similar to that of the experimental points, although the points from both predicted data sets are displaced to the left (lower M), relative to the experimental data. Overall figure 14 suggests that trends can be predicted reasonably well. Using the measured monolith internal dimensions and the Hagen-Poiseuille formulation the non-dimensional pressure drop can be predicted to within about 10% of the experimental results. The predicted maldistribution index, however, can be expected to be between 9% and 17.5% too low.

A simulation has been performed using EQ (1) from Shah(16) as discussed earlier. The results can be compared with those obtained using EQ (2)- the Hagen-Poiseuille equation. The simulations used a grid of 15750 cells and the k-ε RNG turbulence model coupled with the Norris-Reynolds (NR) two-layer wall model. Figure 15 shows the results of these simulations for a 60° diffuser with a uniform inlet velocity profile with *Re* = 61500. The results indicate that even with this new expression the predicted flow maldistribution is little changed.

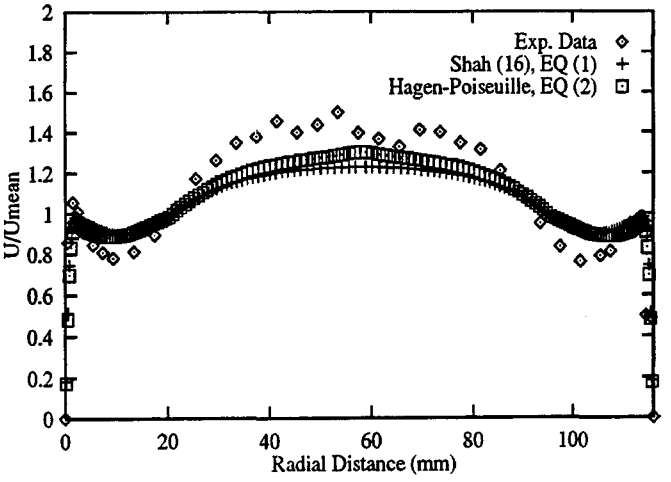

Figure 15: Experimental and predicted (using k-ε RNG and NR models) velocity profiles at rear of monolith for the 60° diffuser, with 152mm monolith, for *Re*=61500 and a uniform velocity profile.

There are several possible explanations for the underprediction of flow maldistribution. These could be associated with either the turbulence model, numerical inaccuracy or monolith resistance formulation. Of these it would seem that the monolith pressure drop expressions that have been used are too simplistic. The flow field at the monolith face is clearly very complex featuring flow with high curvature and presumably

varying levels of turbulence intensity and scale. Presumably there are additional entrance effects and loss factors associated with such a flow field incident on a monolith structure which need to be incorporated into the prescription of the monolith resistance. Further work is clearly needed in order to improve the modelling of the flow at the entrance to the monolith.

CONCLUSIONS

An experimental and theoretical investigation has been performed on the flow and pressure loss in axisymmetric catalytic converters and isolated monoliths under steady, isothermal flow conditions.

Monolith resistance has been measured with a uniform, low turbulence, incident flow field. It has been found that the pressure loss expression for fully developed laminar flow is a good approximation to observations for x^+ greater than 0.2. However, for x^+ less than 0.2 the additional pressure loss due to developing flow is no longer negligible and a better approach is to use the correlation proposed by Shah (16).

From experimental studies on the axisymmetric catalytic converters non-dimensional power law relationships have been derived relating maldistribution and non-dimensional pressure drop to expansion length, *Re*, and monolith length. These expressions are shown to generally fit the data well within ±5%.

CFD predictions of the flow for a wide range of geometric configurations and flow conditions have shown that generally the non-dimensional system pressure loss can be predicted to within about 10% but that the maldistribution index is underpredicted within a range of 9-17.5%. It is believed that the pressure loss expression derived from 1-D flow studies is too simplistic.

CFD predictions do, however, show the same pattern of change as observed experimentally and hence their performance in predicting trends is quite encouraging.

ACKNOWLEDGEMENTS

The authors would like to acknowledge the support from Jaguar Cars Ltd. and Johnson Matthey. In particular Steve Richardson (Jaguar Cars Ltd) and Nigel Will (Johnson Matthey) provided valuable technical assistance on these programmes. Thanks are also expressed to Colin Obray of Coventry University for assistance with the statistical analysis. R. J. Clarkson was supported from a SERC/Jaguar Case award.

REFERENCES

1. Comfort, E. H. "Monolithic catalytic converter performance as a function of flow distribution," ASME Winter Annual Meeting, Paper No. 74-WA/HT-30, 1974.

2. Howitt, J. S. and Sekella, T. C. "Flow effects in monolithic honeycomb automotive catalytic converters," SAE Paper 740244, 1974.

3. Lemme, J. S. and Sekella, T. C. "Flow through catalytic converters-An analytical and experimental treatment," SAE Paper 740243, 1974

4. Lai, M.-C., Kim, J.-Y., Cheng, C.-Y., P., Chui, G. and Pakko, J. D. "Three-dimensional simulations of automotive catalytic converter internal flow," SAE Paper 910200, 1991.

5. Kim, J. Y., Lai, M. C., Li, P. and Chui, G. "Modelling diffuser-monolith flows and its implications to automotive catalyst converter design," SAE Paper 921093, 1992.

6. Bella, G., Rocco, V. and Maggiore, M. "A study of inlet flow distortion effects on automotive catalytic converters," ASME Journ. of Eng. for Gas Turbines and Power, Vol. 113, pp 419-426, 1991.

7. Wendland, D. W., and Matthes, W. R. "Visualisation of automotive catalytic converter internal flows," SAE Paper 861554, 1986.

8. Wendland, D. W., Sorrell, P. L. and Kreucher, J. E. "Sources of monolith catalytic converter pressure loss," SAE Paper 912372, 1991.

9. Wendland, D, W., Matthes, W. R. and Sorrell, P. L. "Effect of header truncation on monolith converter emission-control performance," SAE Paper 922340, 1992.

10. Will, N. S. and Bennet, C. J. "Flow maldistributions in automotive converter canisters and their effect on emission control," SAE Paper 922339, 1992.

11. Weltens, H., Bressler, H., Terres, F., Neumaier, H. and Rammoser, D. "Optimisation of catalytic converter gas flow distribution by CFD predictions," SAE Paper 930780, 1993.

12. Clarkson R. J. "A theoretical and experimental study of automotive catalytic converters," PhD thesis, Coventry University 1995.

13. Schlichting, H. Boundary-Layer Theory, 7th Edition, McGraw-Hill, 1979.

14. Heitor, M. V. and Rodrigues, J. M. "Intercomparison of flow measurements," Technical University of Lisbon, Department of Mechanical Engineering, May 1992.

15. Borger, G.-G., "Optimierung von Windkanaldusen fur den Unterschallbereich-ZfW," vol. 23, pp 45-50, 1975.

16. Shah, R. K. "A correlation for laminar hydrodynamic entry length solutions for circular and noncircular ducts," Journal of Fluids Eng., vol. 100, pp 177-179, June 1978.

17. Computational Dynamics, STAR-CD Users Guide-Version 2.2, 1994.

18. Clarkson, R. J., Benjamin S. F., Girgis, N. S. and Richardson, S. "Theoretical and experimental investigation of the flow in catalytic converters," IMechE Seminar on the Validation of Computational Techniques in Vehicle Design, April 1994.

19. Norris, L. H. and Reynolds, W. C. "Turbulent channel flow with a moving wavy boundary," Report No. FM-10, Department of Mechanical Engineering, Stanford University, 1975.